



A comparative study of batch adsorption process of biomass and its biochar during indigo carmine removal

Imen Ghanmi¹ · Wafa Sassi² · Paula Oulego³ · Sergio Collado³ · Achraf Ghorbal¹ · Mario Díaz³

Received: 28 July 2023 / Revised: 15 October 2023 / Accepted: 21 October 2023
© The Author(s), under exclusive licence to Springer-Verlag GmbH Germany, part of Springer Nature 2023

Abstract

This study is focused on evaluating the effectiveness of raw biomass from pomegranate peels (RPP) and its derived biochar (BPP) for the treatment of dye-containing wastewaters through adsorption. Structural and morphological analyses of RPP and BPP were performed using Fourier transform infrared spectroscopy and scanning electron microscopy. The performance of RPP and BPP as adsorbents for indigo carmine (IC) removal was further investigated in batch mode, the maximum experimental adsorption capacity being 77.87 mg g⁻¹ and 290.04 mg g⁻¹, respectively. The equilibrium data was successfully fitted to the Dubinin-Radushkevich model. The kinetic studies showed that the adsorption of IC was well described by the pseudo-second order, suggesting a chemisorption process onto heterogeneous surface. Various thermodynamic parameters, such as ΔG° , ΔH° , and ΔS° , derived from adsorption data over the temperature range 298 and 328 K, accounted for an endothermic and spontaneous process. A possible adsorption mechanism implying π - π interaction and Van der Waals forces was proposed.

Keywords Pomegranate peels · Biomass · Biochar · Optimization · Adsorption

1 Introduction

The exponential growth of the global population has led to a significant increase in industrialization, particularly in the textile industry [1]. Reports indicate that over 60 billion kilograms of textile products are produced annually worldwide, with each kilogram requiring approximately 200 L of water [2]. Among various dyes used in industries such as textiles, paint, cosmetics, and pharmaceuticals, indigo carmine (IC) is a well-known anionic dye [3, 4].

With socio-economic development, the generation of massive waste has become a pressing issue, posing

challenges for environmental pollution management, as only a fraction of this waste is naturally biodegradable. Consequently, biomass collection and utilization have become crucial concerns. As a result, extensive research has focused on adsorption using different biomass adsorbents for separation and purification purposes. Various experiments utilizing raw eucalyptus bark have been conducted to determine the optimal IC adsorption capacity [5]. Furthermore, investigations on the continuous adsorption-desorption of IC using an invasive macrophyte, *Salvinia minima*, have demonstrated high MB removal rates of 75–78% [6]. Wen et al. [7] achieved an impressive IC adsorption capacity of 370 mg/g using a cationic adsorbent prepared from corn stalk biomass. Conversely, the dried biomass of *Rhizopus oryzae* exhibited lower adsorption capacity, achieving only 50 mg/g of IC removal [8]. In another study, Sen et al. utilized pinecone biomass from *Pinus radiata* and achieved approximately 109.89 mg/g of IC removal at 30 °C [9]. Similarly, Li et al. successfully adsorbed 110.13 mg/g of IC using bulk kitchen waste [10].

In this work, a comprehensive study to compare the performance of two different materials for treating textile dye-containing wastewaters, polluted with IC, was conducted. To that end, raw biomass from pomegranate peels and its derived biochar were tested as adsorbents. A new

✉ Wafa Sassi
wafa.sassi@issatgb.u-gabes.tn

¹ Research Unit Advanced Materials, Applied Mechanics, Innovative Processes and Environment, UR22ES04, Higher Institute of Applied Sciences and Technology of Gabes, University of Gabes, Avenue Omar Ibn Khattab, 6029 Gabes, Tunisia

² Faculté des Sciences, Unité de Recherche Électrochimie, Matériaux et Environnement UREME (UR17ES45), Université de Gabès, 6000 Gabès, Tunisia

³ Department of Chemical and Environmental Engineering, University of Oviedo, E-33071 Oviedo, Spain

optimization model using the central composite design (CCD) to evaluate the technical aspects of both materials was used. Additionally, the kinetics, isotherms, and thermodynamic behaviors of these adsorbents were also studied to gain a deeper understanding of the adsorption process and the possible mechanism.

2 Experimental

2.1 Materials and apparatus

In this study, we utilized various analytical instruments and techniques to investigate the properties of the samples. The ultra-violet (UV) spectrophotometer mentioned in this paper has been previously referenced in works by Sassi et al. [11, 12]. For elemental analysis, a high-resolution compact scanning electron microscope (SEM) of the third generation, manufactured by HITACHI and model FlexSEM1000 II, was employed [11, 12]. To ensure empirical comparison, both the raw perlite and the samples were subjected to the same conditions. They were mixed with water under optimal parameters such as acidity (pH), contact time (t min), dye content (C mg/L), and temperature (T K). Subsequently, the mixture was filtered, washed, and dried.

2.2 Preparation of biomass and its derived biochar

The sample collection of the pomegranate fruit variety “*Punica granatum*” was conducted in Tunisia, in the Gabes region (in Kattena) during the month of October 2022. Raw pomegranate peels (RPP) were collected and then cleaned multiple times with running water to remove dust and small microorganisms. Afterwards, the material was cut into small pieces and immersed in water for 24 h until the peels color disappeared. The well-washed RPP were dried in an oven at 50 °C for 24 h. After 24 h of drying, the RPP were further cut into smaller pieces and then ground. Subsequently,

they were passed through a sieve with a particle size of 212 μm . The choice of this small particle size of 212 microns is to achieve the best possible adsorption. According to Lima et al. [13], this property plays a crucial role in elucidating the material’s performance in adsorbing dye molecules because surface textural characteristics are significant factors in the adsorption process. The ground and sieve pomegranate peels were washed with distilled water until the water became clear in order to remove impurities and dust. Subsequently, this material underwent drying in an oven at a temperature of 100 °C for 24 h. After drying, the adsorbent was ground into a fine powder using a grinder, and then the nanoparticles underwent calcination in a furnace at 1000 °C. The carbonization process is considered complete after 2 h. The obtained paste was gradually cooled and then frozen at -4 °C, followed by lyophilization. Finally, the biochar is ready as a dry powder.

Figure 1 illustrates the steps involved in preparing our materials.

2.3 Methods and reagents

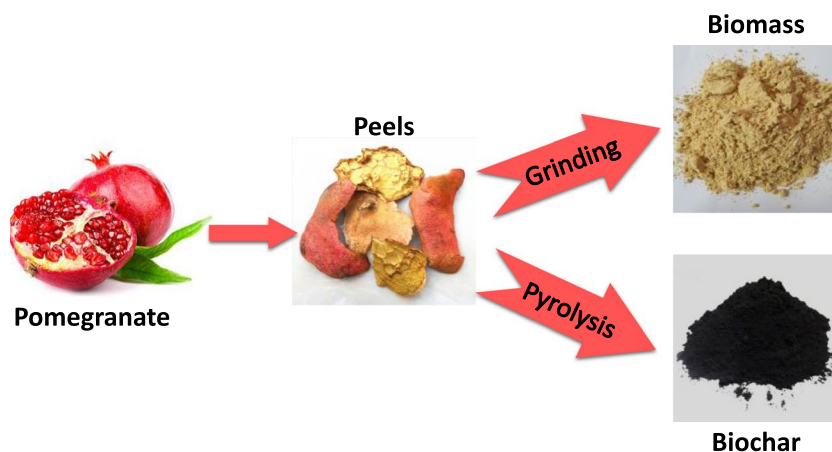
The optimization process was carried out using the STATISTICA software program (Version 12.4 November 2018, USA). The model used was the CCD with five levels ($-\delta$, -1 , 0 , $+1$, $+\delta$) with binary response tools and three factors (contact time, dye concentration, and temperature) [12, 14].

All chemicals and dyes were procured from Sigma-Aldrich. The hazardous dye investigated in this study is the IC. The formula and UV spectra of this dye are deeply presented in the supplementary data.

2.4 Adsorption experiments

Batch experiments were carried out to assess the adsorption performance. The study investigated the impacts of different initial concentrations of IC.

Fig. 1 Materials origin and preparation



The remaining IC concentrations in the solution were measured using UV-visible spectrometry (UV-1800, Metrometer, France). The removal efficiency (RE) was calculated using the following formula:

$$RE = 100 \times \frac{(C_0 - C_e)}{C_0} \tag{Eq. 1}$$

Here, C_0 and C_e represent the initial and equilibrium IC concentrations (mg/L) in the solution at t_0 and t_e , respectively.

3 Results and discussion

3.1 The pH_{zc} parameter

The pH at the point of zero charge (pH_{pzc}) refers to the pH value where the surface charge of a material is neutral. In the case of our materials, Fig. 2 illustrates how the pH at the end of a process (pH_{final}) changes with the initial pH ($pH_{initial}$).

The pH_{pzc} values for RPP and BPP materials were determined to be 4.12 and 7.56, respectively. When the pH was below the pH_{pzc} , the surface of the adsorbent carried a positive charge, promoting the adsorption of anionic dyes, as demonstrated by Sassi et al. [12]. Conversely, when the pH

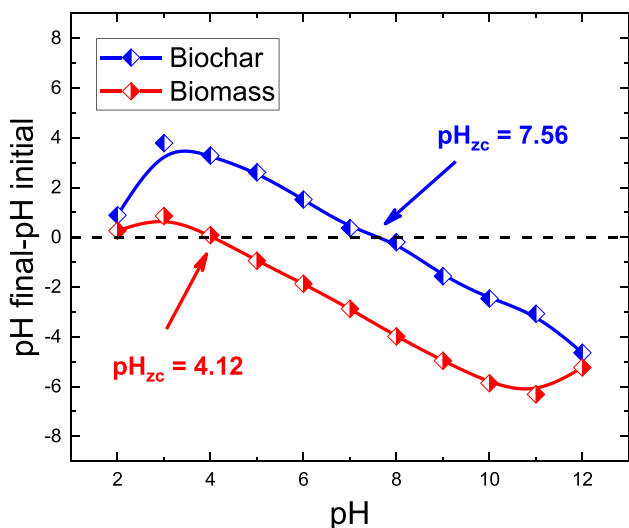


Fig. 2 Surface pH variation as a function of solution $pH_{initial}$ of RPP and BPP

exceeded the pH_{pzc} , the adsorbent surface became negatively charged, favoring the adsorption of cationic dyes. In this study, the contaminant being investigated was IC, which is an anionic dye. Consequently, the highest adsorption capacities of both materials RPP and BPP were observed in an acidic pH range, specifically at pH = 3.0. The effect of pH is primordial for CI removal success. In fact, the highest removal is always recorded for anionic dyes at pH range when the material is positive charged (i.e., pH = 3).

3.2 CCD optimization model

In this study, we utilized STATISTICA 12.8.0 software to analyze the adsorption of IC (insert compound) onto pomegranate peels. To optimize the process, we employed the CCD model and response surface methodology (RSM), aiming to determine the optimum conditions for several factors under investigation. By implementing RSM based on the CCD, we were able to minimize the number of experiments, as previously reported by Diao et al. [15]. Following the recommendations of Sassi et al. [16] and Pils and Laired [17], the impact of each studied factor, as well as their interactions, on the adsorption yield (Y%: adsorption yield) was evaluated using CCD. For the selected factors, namely contact time, IC concentration, and the media temperature, the experimental field is outlined in Table 1.

δ is the code of rotatability and orthogonality for the adopted CCD calculated using Eq. 2 [18]:

$$\delta = \sqrt{\frac{n_f \times (\sqrt{n} - \sqrt{n_f})^2}{4}} \tag{Eq. 2}$$

where n_f is the number of runs proposed by the factorial plan (Eq. 3), and n is the total number of runs suggested by the CCD model, explained in Eq. 4 [16]:

$$n_f = l^3 \tag{Eq. 3}$$

$$n = n_f + l \times 3 + c \times r \tag{Eq. 4}$$

where l is the level, c is the number of model centers, and r is its repetition number. In our case, n and the code δ are 16 runs and 1.69, respectively. The equivalency between the design codes and factor values was presented by Sassi et al. [16]; the error analysis is detailed in the supplementary data, and the adsorption yield was calculated using Eq. 5:

Table 1 Experimental field for the studied factors

Factors	Code	(- δ)	(-1)	(0)	(+1)	(+ δ)
Contact time t_c (min)	X_1	1.32	32	77	122	152.68
IC concentration C (mg/L)	X_2	6.14	30	65	100	123.82
Temperature (K)	X_3	294.36	308	328	348	361.64

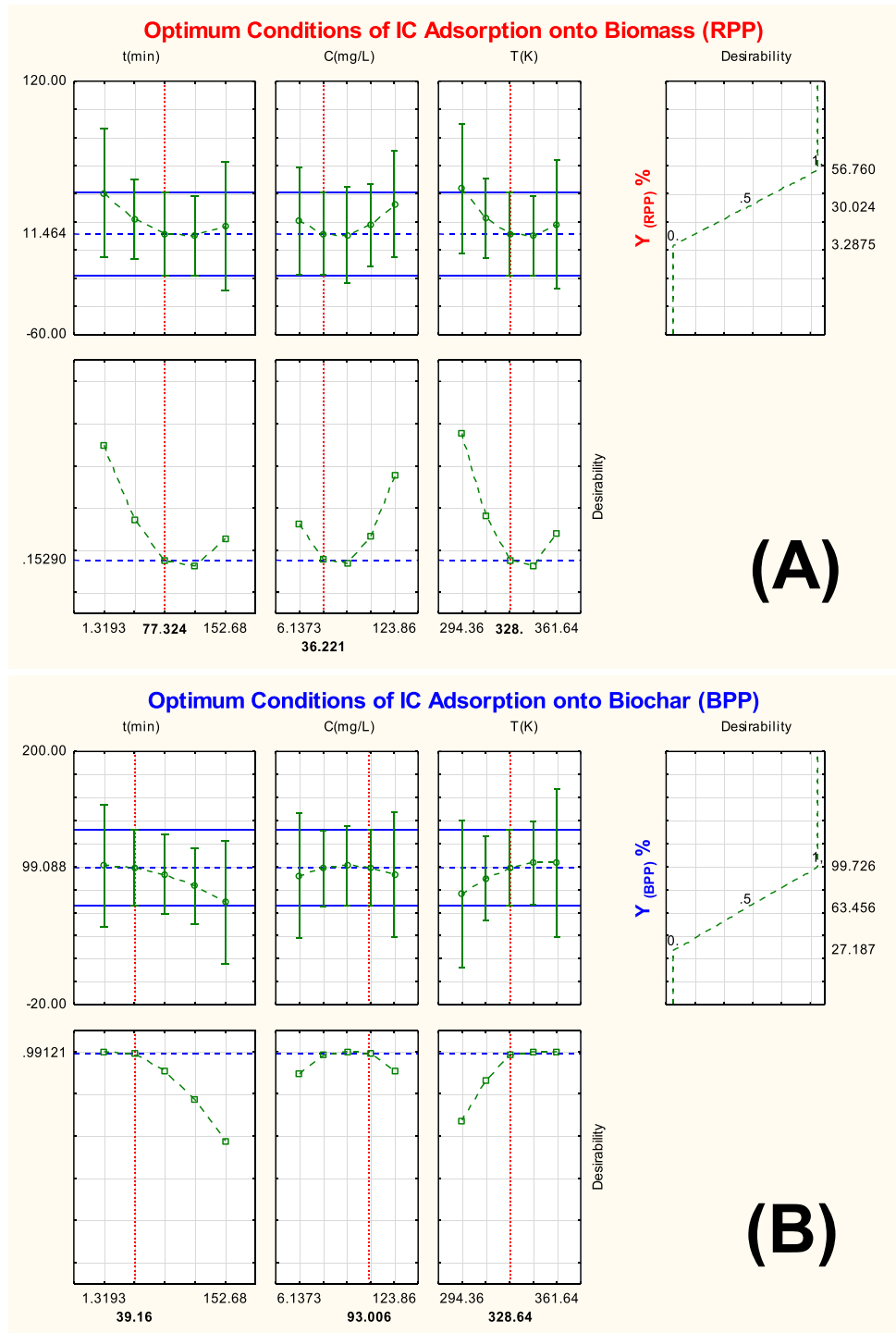
$$Y (\%) = \frac{C_{ads}}{C_0} \times 100 \quad (\text{Eq. 5})$$

To compare and optimize the IC adsorption yields onto the biomass (raw pomegranate peels) and its derived biochar, a binary compilation of the CCD model has been applied.

The optimum conditions generated by the software are presented in Fig. 3.

The CCD model generated optimum conditions for both materials, with a contact time (t_c) of 77 and 39 min, an IC concentration of 36 and 93 mg/L, and media temperature of 328 K for biomass and biochar, respectively. These optimal conditions will be adopted for all the subsequent tests. The experimental design successfully demonstrated the effectiveness of each factor within the experimental domain. At these optimum conditions, the adsorption yields were found to be

Fig. 3 Optimum conditions of the IC adsorption onto pomegranate peels **A** biomass (RPP) and **B** biochar (BPP)



55% for the biomass and 99% for the biochar, indicating a higher removal percentage compared to other studies that used spontaneous adsorption on agricultural waste biomass or multi-wastes biochar compounds. Indeed, Lee et al. [19] achieved a value of 86% adsorption of fluor, while Cai et al. [20] only eliminated 88% of aniline vapor using the biomass adsorbent. The mathematical prediction model, represented by Eqs. 6, 7, provides a means of predicting yields for future experiments in this field:

$$Y_{RPP}(\%) = (30.02) - (5.37 \times X_1) + (3.61 \times X_2) - (3.75 \times X_3) + (2.01 \times X_1X_2) - (1.28 \times X_1X_3) + (2.55 \times X_2X_3) + 4.25 \quad (\text{Eq. 6})$$

$$Y_{BPP}(\%) = (63.46) - (10.22 \times X_1) + (1.06 \times X_2) - (3.74 \times X_3) + (1.25 \times X_1X_2) - (1.96 \times X_1X_3) + (2.45 \times X_2X_3) + 4.86 \quad (\text{Eq. 7})$$

However, there were limitations in the predictive modeling process. It was evident that the contact time significantly influenced the adsorption yields for both materials. The impact of contact time and temperature appeared to be inversely proportional to the response since the a_1 is negative for both materials. Furthermore, the coefficient values for the dye's concentration factor were positive, indicating a directly proportional effect. All interaction coefficient values were less than the residual ($\Delta y = 4.25$ and 4.86 for the RPP and BPP, respectively). This observation may neglect the effect of interaction between factors for both materials.

The effectiveness of the CCD model was demonstrated by its ability to accurately predict values for both materials, as shown in Fig. 4, which displayed a good fit between the experimental and predicted results.

The effectiveness of the adsorption process modelization for both materials can be observed in Fig. 4. It is evident that the CCD model is well-suited for representing the adsorption process for both the biomass and the biochar. This is supported by the regression coefficients R^2 , which were found to be 0.9819 and 0.9687 for the biomass and the biochar, respectively, indicating a strong correlation between the model and the experimental data.

Furthermore, Fig. 4 provides additional insights. It shows that the adsorption yield's mean for the biomass falls within a relatively low range, spanning from 10 to 50%. On the other hand, the biochar exhibits a significantly higher adsorption yield's mean, ranging from 55 to 99%. These findings clearly indicate that the adsorption capacity of the biochar surpasses that of its original biomass. In summary, the results presented in Fig. 4 provide strong evidence supporting the superiority of the biochar in terms of adsorption capacity when compared to its biomass precursor.

In the rest of this study, all experiments will be conducted under the optimal conditions determined by the CCD model generated using STATISTICA software.

3.3 Batch adsorption process

The biomass and derived biochar were used to apply a treatment to a colored wastewater with IC dye. At this stage, a new parameter is used to evaluate the IC removal, which is the adsorption capacity, calculated using Eq. 8:

$$Q_{(mg/g)} = \frac{C_{ads}}{C_0} \times \frac{V}{m} \quad (\text{Eq. 8})$$

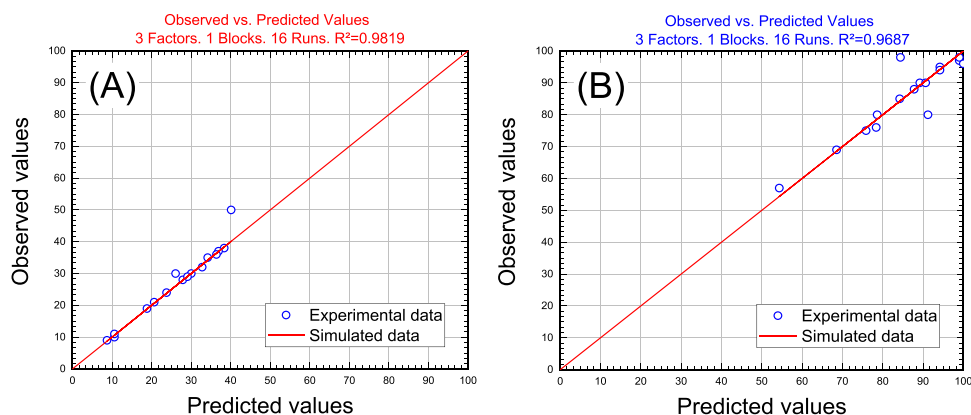
where the concentrations of IC in the solution, represented by C_0 (initial concentration) and C_e (equilibrium concentration) in milligrams per liter (mg/L), were determined in relation to the adsorbent mass (g) and the solution volume (L). At the optimum conditions, the respective amounts of IC adsorbed were 137.5 mg/g for the biomass and 247.5 mg/g for the biochar, corresponding at 55 and 99% of RE, respectively.

In order to study the adsorption mechanism, kinetic, isotherm, and thermodynamic studies were occurred.

3.3.1 Kinetic studies

Figure 5 shows the evolution of the adsorption capacity function of contact time.

Fig. 4 Linearity test between predicted and observed responses values of the IC adsorption yields pomegranate peels **A** biomass and **B** biochar



As depicted in Fig. 5, the biomass exhibits a slow kinetic adsorption of IC dye. It is noteworthy that the maximum Q_t was attained after approximately 60 min of contact time. Conversely, the biochar demonstrates a faster adsorption capacity, reaching its maximum within the initial 40 min. Another intriguing observation is that the theoretical Q_t

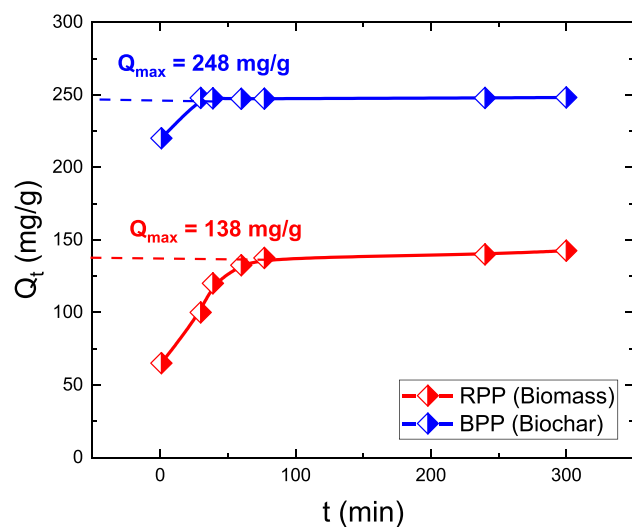
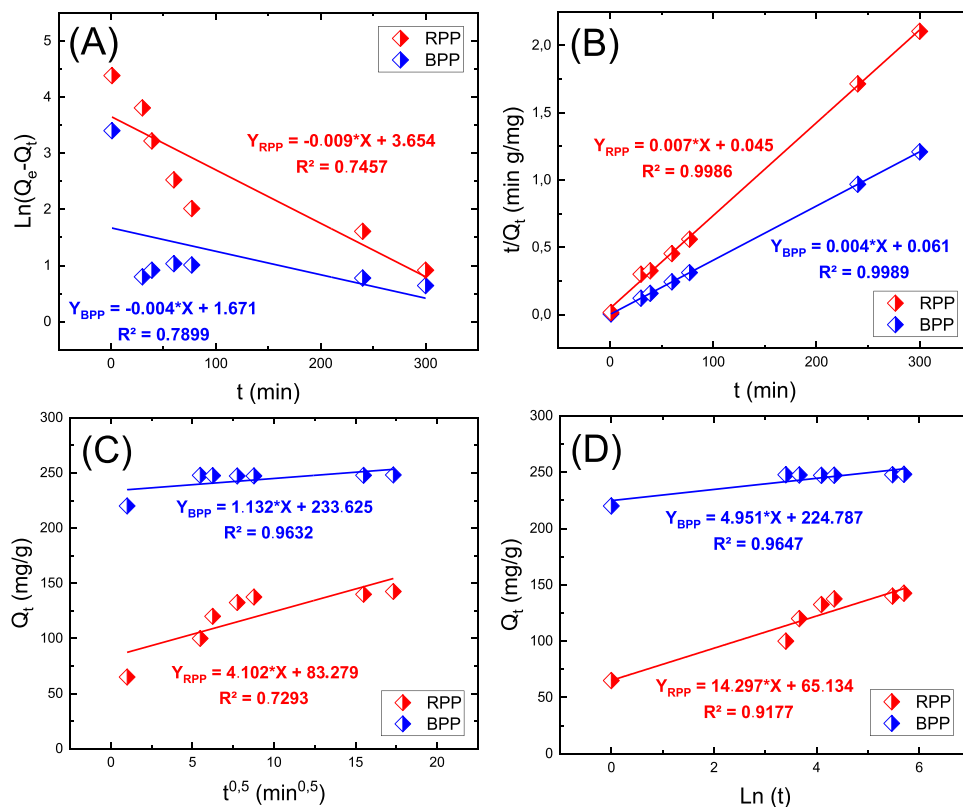


Fig. 5 Adsorption capacity evolution of IC dye onto pomegranate peels biomass (RPP) and biochar (BPP) function of contact time

Fig. 6 Kinetic linear modelization of the IC adsorption onto RPP and BPP **A** PFO, **B** PSO, **C** IPD, and **D** Elovich (pH = 3, T = 328 °K)



values were 138 mg/g and 248 mg/g for the RPP and BPP, respectively.

Purpose to understand the kinetic mechanism of RPP and BPP during the IC adsorption, some kinetic models were applied, and their equations are detailed in the supplementary data.

Figure 6 and Table 2 gather the pseudo-first order (PFO), the pseudo-second order (PSO), the intra-particle diffusion (IPD), and the Elovich models.

The investigation of Fig. 6 and Table 2 shows that the regression coefficients (R^2) of the PSO and Elovich kinetic models were close to unity for both materials. The first model suggests that the adsorption rate is influenced not only by the dye's concentration in the liquid phase but also by the material's adsorption capacity [21]. Furthermore, the Elovich kinetic model appears to fit well with the adsorption process of IC onto pomegranate peels biomass and biochar, with R^2 values of 0.9177 and 0.9647, respectively. The model's parameter β provides an estimated value for the desorption rate of IC dye from RPP and BPP. The low β values of 0.069 and 0.202 g/mg for RPP and BPP materials, respectively, confirm that the IC adsorption process is not spontaneously reversible. The adsorption process mechanism will be detailed in the next section with the isothermic study.

Table 2 PFO, PSO, IPD, and Elovich parameters and model correlation coefficients

	Pseudo-first order (PFO)			Pseudo-second order (PSO)		
	k_{PFO} (min ⁻¹)	Q_e (mg g ⁻¹)	R^2	k_{PSO} (mg g ⁻¹ min ⁻¹)	Q_e (mg g ⁻¹)	R^2
RPP	0.009	38.63	0.7457	0.001	142.86	0.9986
BPP	0.004	5.32	0.7899	0.001	250.05	0.9989
	Intra-particle diffusion (IPD)		Elovich			
	k_{IPD} (mg g ⁻¹ min ^{-0.5})	R^2	β (g mg ⁻¹)	α (mg g ⁻¹)	R^2	
RPP	4.102	0.7293	0.069	135.68	0.9177	
BPP	1.132	0.9632	0.202	247.99	0.9647	

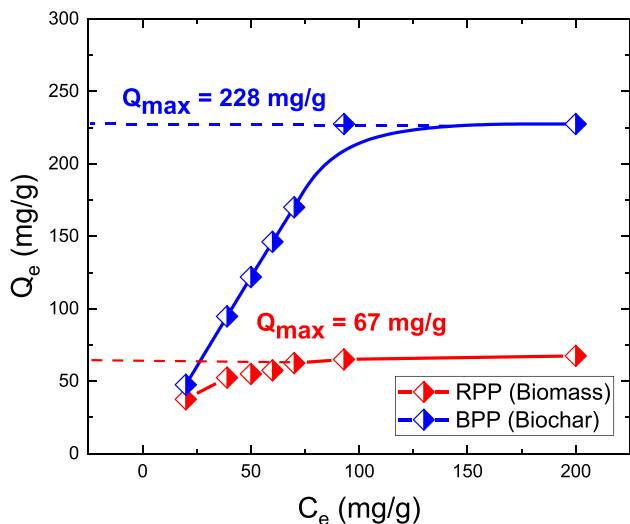


Fig. 7 IC adsorption capacity evolution onto pomegranate peels biomass (RPP) and biochar (BPP) function of equilibrium dye concentration

3.3.2 Isotherm studies

Figure 7 depicts the change in adsorption capacity over IC concentration.

As shown in Fig. 7, the saturation of biochar is twice as large as that of pomegranate peels biomass. Specifically, the biochar (BPP) reached a saturation point (Q_{max}) of 228 mg/g starting from the IC dye concentration of 100 mg/L, whereas the pomegranate peels biomass (RPP) saturated earlier at the Q_{max} of 67 mg/g. This result confirms that the BPP possesses a higher adsorption capacity compared to the RPP.

Figure 8 and Table 3 gather the Langmuir, Freundlich, Temkin, and Dubinin-Radushkevich (D-R) isotherm models.

Various isotherms were tested to investigate the mechanism of IC adsorption onto pomegranate peels biomass and biochar. The four isotherms with higher regression coefficients (R^2) were selected, namely Langmuir, Freundlich, Temkin, and D-R. All of these isotherms exhibited R^2 values greater than 0.91.

Firstly, according to Lima et al. [22, 23], the Langmuir isotherm suggests monolayer adsorption with a unique type

of interaction between the adsorbent and adsorbate (surface homogeneity) [24]. The isotherms interpretation has been enhanced according to the work of Dos Reis et al. [25, 26]. Additionally, the Freundlich isotherm proposes multilayer dye adsorption with a heterogeneous surface. Furthermore, the Temkin model indicates that the IC dye adsorption occurs within the pores of both materials. Finally, the D-R isotherm introduces a parameter that is proportional to the adsorption heat. Indeed, if this parameter, denoted as ΔE , is lower than 8 kJ/mol, the adsorption is considered physical. However, if ΔE exceeds 8 kJ/mol, it suggests a chemisorption process. In our case, the ΔE values were found to be 13.89 kJ/mol and 20.33 kJ/mol for pomegranate peels biomass and biochar, respectively. This result suggests a chemical IC dye adsorption process for both RPP and BPP materials, which will be further confirmed by a thermodynamic study.

3.3.3 Thermodynamic studies

The Van't Hoff method was employed to estimate the thermodynamic parameters. In recent studies by Lima et al. [22, 23, 27], the expression for the thermodynamic equilibrium constant for adsorption (K_e°) was calculated. The authors deduced the following expression for the dimensionless thermodynamic equilibrium constant [28, 29]:

$$K_e^\circ = \frac{Q_e}{C_e} = \frac{K_e}{\gamma} = \frac{(1000 \cdot K_g \cdot M_{IC} [IC]^\circ)}{\gamma} \tag{Eq. 9}$$

where γ is the activity, M is the IC molecular weight (466 g/mol), and K_e is the best fitted isotherm.

$$\Delta G^\circ = -R T \ln K_e^\circ \tag{Eq. 10}$$

$$K_e^\circ = \exp\left(-\frac{\Delta G^\circ}{R T}\right) \tag{Eq. 11}$$

$$\Delta G^\circ = \Delta H^\circ - T \Delta S^\circ \tag{Eq. 12}$$

$$K_e^\circ = \exp\left(-\frac{\Delta H^\circ}{R} \times \frac{1}{T} + \frac{\Delta S^\circ}{R}\right) \tag{Eq. 13}$$

Fig. 8 Isotherm linear modelization of the IC adsorption onto RPP and BPP **A** Langmuir, **B** Freundlich, **C** Temkin, and **D** Dubinin-Radushkevich (D-R) (pH = 3, T = 328 °K)

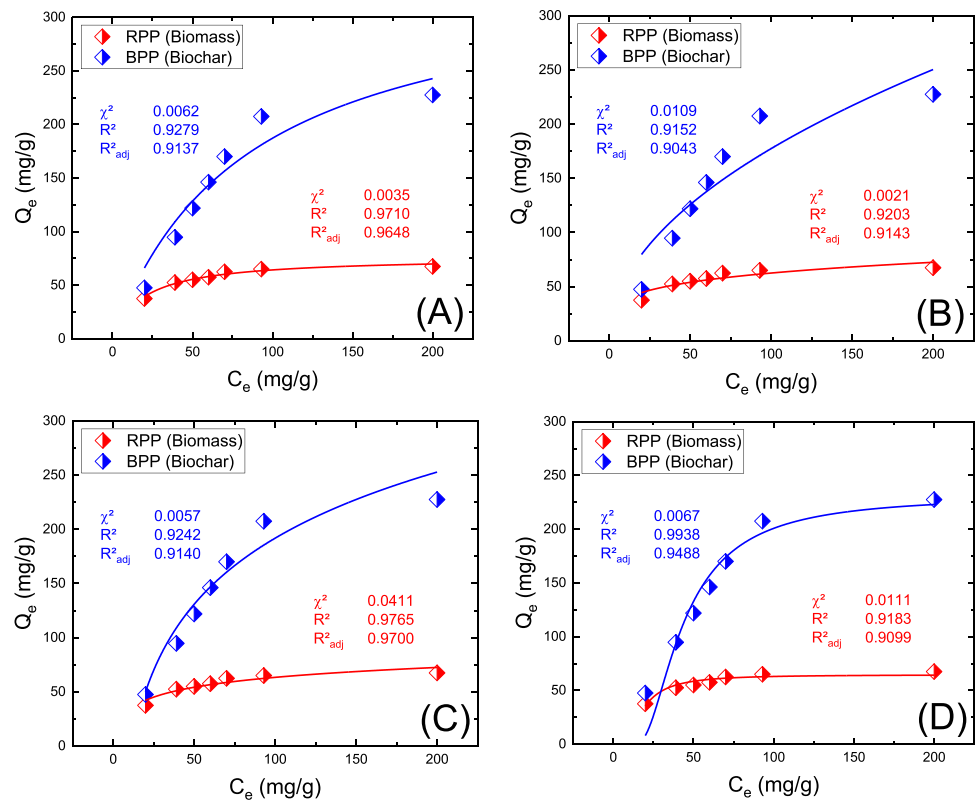


Table 3 Langmuir, Freundlich, Temkin, and Dubinin-Radushkevich parameters and model correlation coefficients

	Langmuir			Freundlich		
	k_L (min ⁻¹)	Q_m (mg g ⁻¹)	R^2	k_F (mg g ⁻¹ L ^{1/n})	n	R^2
RPP	0.566	76.97	0.9710	13.22	2.88	0.9203
BPP	0.012	333.30	0.9279	1.33	56.07	0.9152
	Temkin			Dubinin-Radushkevich		
	k_T (L mg ⁻¹)	ΔE (kJ mol ⁻¹)	R^2	ΔE (kJ mol ⁻¹)	Q_s (mg g ⁻¹)	R^2
RPP	0.263	23.02	0.9765	14.19	77.87	0.9183
BPP	0.282	24.17	0.9242	19.89	290.04	0.9938

$$\ln K_e^\circ = \left(-\frac{\Delta H^\circ}{R} \right) \frac{1}{T} + \frac{\Delta S^\circ}{R} \quad (\text{Eq. 14})$$

Figure 9 illustrates the changes in adsorption capacity with varying temperatures and is presented in the Van't Hoff plot.

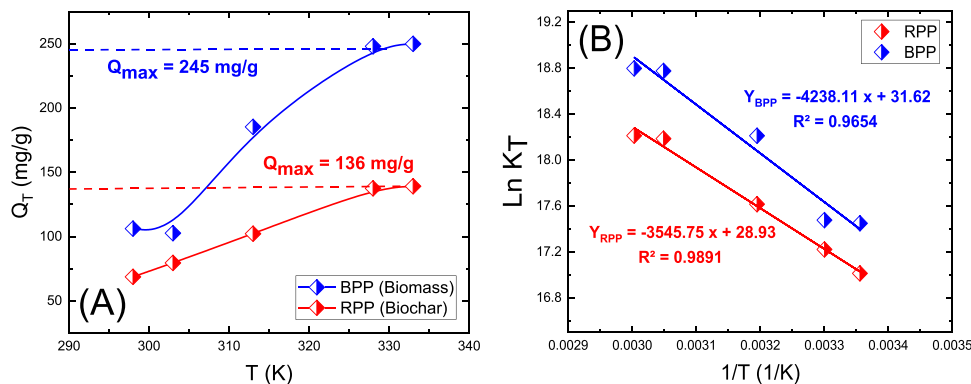
The graph depicted in Fig. 9A indicates that as the temperature increases, the adsorption quantities also increase. This suggests a proportional relationship between reactor temperature and the amount of adsorbed material, confirming the endothermic nature of IC adsorption onto both biomass and biochar as previously suggested. The higher adsorption capacity at elevated temperatures may be attributed to the enlargement of pore size and/or activation of the nano-adsorbent surface [30]. It is noteworthy that the selectivity ratio favors IC adsorption, with recorded maximum capacities (Q_{\max}) of 136 mg/g for RPP

and 245 mg/g for BPP. These findings further confirm that the optimal condition for the process is the pH of 3.

Figure 9B presents Van't Hoff curves with regression coefficients (R^2) of 0.9891 for RPP and 0.9654 for BPP, respectively. The close proximity of these values to unity indicates that the Van't Hoff method can effectively predict the thermodynamic parameters of the IC adsorption process. The thermodynamic parameters obtained using Eq. 12 and Eq. 14 are listed in Table 4.

It is important to highlight that the negative values of ΔG° confirm the spontaneous nature of the IC dye adsorption processes. Additionally, the positive value of ΔH° for both material RPP and BPP (29.48 and 35.24 kJ/mol, respectively) indicates that the IC adsorption process is endothermic. Moreover, both enthalpy values are above 20 kJ/mol, suggesting that chemical adsorption takes place [31, 32]. Moreover, the positive values of ΔS° for both adsorbents

Fig. 9 **A** Evolution of IC dye adsorption capacity as a function of temperature (pH = 3) and **B** the Van't Hoff curve of RPP and BPP



indicate an increase in surface randomness and disorder [33, 34]. This further confirms the occurrence of chemisorption. These results align with the findings of the kinetic and isotherm studies.

3.4 Adsorption characterization and mechanism

3.4.1 SEM characterizations

The biomass and biochar morphologies before and after IC adsorption were investigated by SEM. The micrographs are presented in Fig. 10.

Figure 10A and B depict the morphologies of pomegranate peels biomass (RPP) and biochar before and after adsorption of the IC dye. The RPP exhibits organic particles with a lignocellulosic form. Upon pyrolysis and the breakdown of cellulose, hemicellulose, and lignin compounds, the biochar displays a more pronounced appearance with surface pores. The adsorption of the IC dye brings about transformations on the surface of both RPP and BPP. The biomass particles agglomerate and become swollen, indicating the successful adsorption of IC. Furthermore, the biochar loses its surface pores and regularity, possibly suggesting a change in its structural composition.

3.4.2 FTIR characterizations

The biomass and biochar before and after adsorption have been analyzed using FTIR analysis. The spectra of all samples were added in Fig. 11. The carmine indigo

Firstly, the comparison between biomass and biochar spectra (Fig. 11A and B) shows that the pyrolysis breaks down the complex organic molecules present in biomass into simpler compounds. Indeed, this process can result in the release of volatile gases, such as methane, carbon dioxide, and various organic compounds, leaving behind the biochar solid residue. Moreover, the pyrolysis generally [35–39] reduces the content of heteroatoms like oxygen, nitrogen, and sulfur in the biomass. This results in a higher carbon content in the remaining material. The analysis of Fig. 11A and B (the CI spectrum) shows the characteristic bands. Firstly, the bands around 3300 cm^{-1} are associated with vibrations of hydroxyl groups (-OH). Moreover, bands around 1700 cm^{-1} are associated with vibrations of carbonyl (C=O) groups. All these bands are present in the RPP and BPP spectra confirming the adsorption of CI onto these materials.

These observations provide confirmation of the IC dye adsorption onto both the biomass and its biochar materials.

3.4.3 IC dye adsorption mechanisms

Based on the results obtained below, the mechanism of pomegranate peels biomass and biochar during IC dye adsorption can be estimated. The proposed mechanism is illustrated in Fig. 12.

To gain a better understanding of the interaction strength between the IC and either RPP or BPP, a proposed mechanism is suggested in Fig. 12.

Table 4 Thermodynamic parameters of the IC adsorption process onto pomegranate peels biomass and biochar

Temperature (°K)	Pomegranate peels biomass (RPP)			Pomegranate peels biochar (BPP)		
	ΔG° (kJ mol ⁻¹)	ΔH° (kJ mol ⁻¹)	ΔS° (J mol ⁻¹ K ⁻¹)	ΔG° (kJ mol ⁻¹)	ΔH° (kJ mol ⁻¹)	ΔS° (J mol ⁻¹ K ⁻¹)
298	-46.39351	+29.48	240.52	-47.58237	+35.24	262.89
303	-46.96075			-47.6574		
313	-48.03558			-49.65923		
328	-49.59113			-51.19914		
333	-49.66174			-51.25907		

Fig. 10 SEM micrographs before IC adsorption onto the dried particles of pomegranate peels biomass (A) and biochar (B) and after adsorption (C, D) at optimum conditions (pH = 3, T = 328 K)

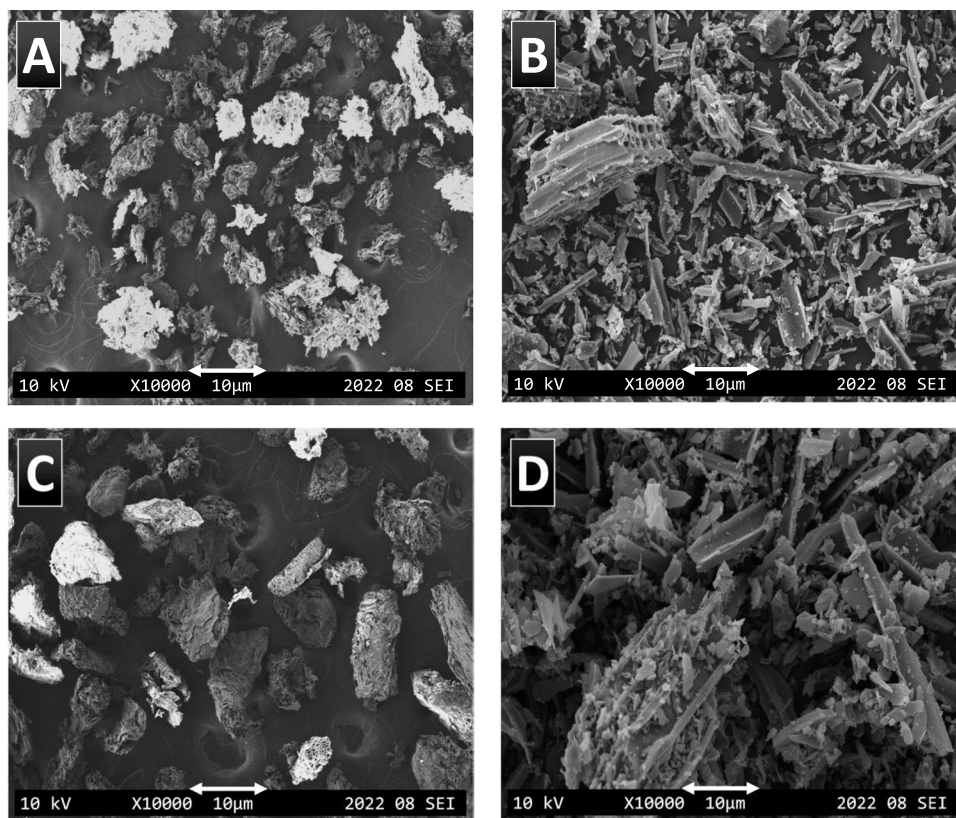
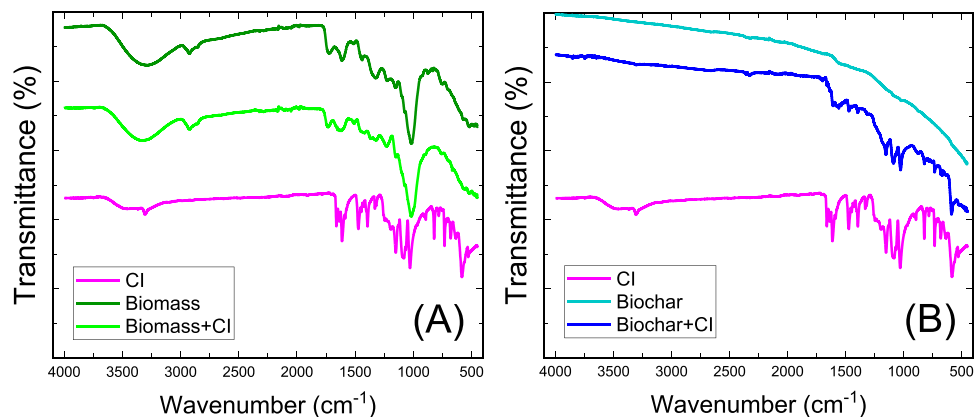


Fig. 11 FTIR spectra before and after IC adsorption onto the dried particles of pomegranate peels A biomass and B biochar at optimum conditions (pH = 3, T = 328 K)



It should be noted that a smaller ΔE corresponds to a shorter bond length and a stronger interaction force [40]. Furthermore, literature [41] revealed that the interaction force between N-H-N involved π - π interaction and Van der Waals forces displayed as a green color in Fig. 12. The interaction forces between other functional groups appeared red, indicating hydrogen bonding [40, 41]. These findings align with our hypothesis support the proposed adsorption models. In addition, the ΔE_{ad} values (adsorption energy), calculated in the isotherm models, further confirming that -COOH and -OH are the primary adsorption functional groups [42].

Additionally, this bonding provides the endothermic nature of IC-RPP and IC-BPP adsorption as observed in the experimental results.

3.5 Literature comparison of Cl removal using a biomass and its biochar

In order to evaluate the impact of utilizing biochar in lieu of biomass, Table 5 provides a comparative overview of IC adsorption capacities across different materials as reported in the existing literature.

Fig. 12 Interaction mechanism between the IC dye molecules and the pomegranate peels biomass and biochar during the adsorption process at generated optimum conditions (pH = 3, T = 328 K)

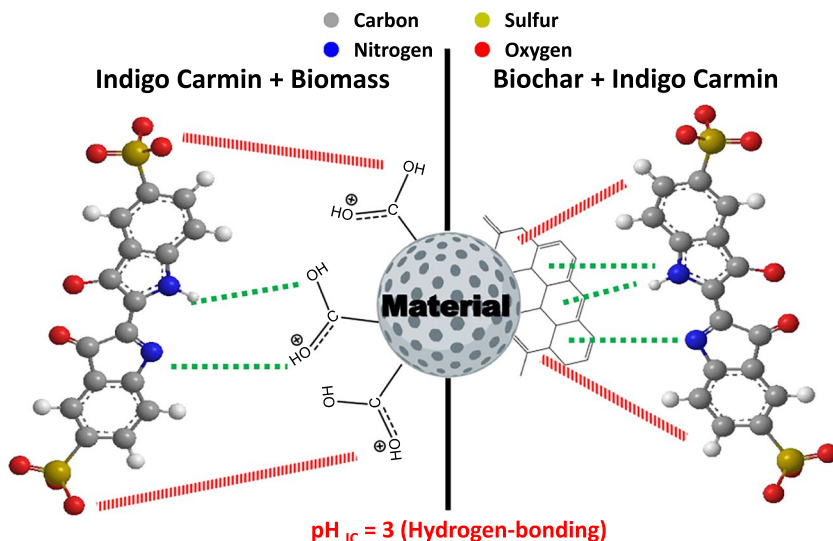


Table 5 Literature comparison of pollutant removal using a biomass and its derivative biochar

Pollutant	Adsorbent	Biomass adsorption capacity (mg/g)	Biochar adsorption capacity (mg/g)	References
CO ₂	Wood waste	56.22	72.42	[43]
Zinc (II)	Straw waste	2.06	22.01	[44]
Sodium	Agricultural biomass	15.5	33.9	[45]
Methylene blue	Vascular plant	217.11	953.53	[46]
Methylene blue	Fly ash	71.22	854.75	[47]

4 Conclusion

Raw biomass of pomegranate peels (RPP) and the resulting biochar (BPP) can be considered suitable adsorbents for the removal of dye-containing wastewaters. The pH of the zero-charge point (pH_{zc}) of RPP and BPP were significantly different with values of 4.12 and 7.56, respectively. The optimal contact times required to achieve maximal adsorption efficiency were 77 min for RPP and 39 min for BPP. Furthermore, the optimal temperature was identified as 328 K for both materials, indicative of an endothermic nature of the adsorption process. Under these optimized conditions, the respective dye REs were measured at 55% for RPP and an 99% for BPP. FTIR and SEM analyses have proved the adsorption of the dye onto the surfaces of both RPP and BPP materials. Additionally, mechanism of adsorption, which involved π-π interaction and Van der Waals forces, has been proposed.

Supplementary Information The online version contains supplementary material available at <https://doi.org/10.1007/s13399-023-05045-4>.

Author contributions The contribution of each author is listed as follows:

✓ IG: conceptualization, software, investigation, methodology, writing, and editing

- ✓ WS: methodology, writing, and editing
- ✓ PO: methodology, writing, and editing
- ✓ SC: analysis and interpretations
- ✓ AG: supervision and review
- ✓ MD: supervision and review

Funding P.O., S.C., and M.D. are grateful for the financial support from the Science, Innovation and University Office of the Principality of Asturias (Spain) through the project GRUPIN AYUD/2021/51041. W.S. would like to thank the Tunisian Ministry of Higher Education and Scientific Research under the Project Code (22PEJC-D1P3) for funding.

Data availability Supplementary data is available.

Declarations

Ethical approval All the authors deliberately approved the ethical rules adopted by the journal.

Consent to participate All the authors expressed their solemn agreement to participate in the conception and elaboration of this work.

Consent to publish All the authors deliberately consent to publish this work.

Competing interests The authors declare no competing interests.

References

- Amin MT, Alazba AA, Shafiq M (2019) Comparative study for adsorption of methylene blue dye on biochar derived from orange peel and banana biomass in aqueous solutions. *Environ Monit Assess* 191:735. <https://doi.org/10.1007/s10661-019-7915-0>
- Chauhan K, Tiwari RK (2020) Study of thermomechanical properties of glycidoxypopyl trimethoxy silane functionalized nanosilica/amine terminated poly (butadiene-co-acrylonitrile) rubber modified novolac epoxy composites for high performance applications. *J Polym Res* 27:319. <https://doi.org/10.1007/s10965-020-02278-z>
- Yagub MT, Sen TK, Afroze S, Ang HM (2015) Fixed-bed dynamic column adsorption study of methylene blue (MB) onto pine cone. *Desalination. Water Treat* 55:1026–1039. <https://doi.org/10.1080/19443994.2014.924034>
- Afroze S, Sen TK, Ang HM (2016) Adsorption performance of continuous fixed bed column for the removal of methylene blue (MB) dye using Eucalyptus sheathiana bark biomass. *Res Chem Intermed* 42:2343–2364. <https://doi.org/10.1007/s11164-015-2153-8>
- Ahmad MB, Soomro U, Muqet M, Ahmed Z (2021) Adsorption of indigo carmine dye onto the surface-modified adsorbent prepared from municipal waste and simulation using deep neural network. *J Hazard Mater* 408:124433. <https://doi.org/10.1016/j.jhazmat.2020.124433>
- Pérez-Morales JM, Sánchez-Galván G, Olguín EJ (2019) Continuous dye adsorption and desorption on an invasive macrophyte (*Salvinia minima*). *Environ Sci Pollut Res* 26:5955–5970. <https://doi.org/10.1007/s11356-018-04097-8>
- Wen X, Yan C, Sun N, Luo T, Zhou S, Luo W (2018) A biomass cationic adsorbent prepared from corn stalk: low-cost material and high adsorption capacity. *J Polym Environ* 26:1642–1651. <https://doi.org/10.1007/s10924-017-1072-8>
- Dey MD, Shukla R, Bordoloi NK, Doley R, Mukhopadhyay R (2015) Mechanism of adsorptive removal of methylene blue using dried biomass of *Rhizopus oryzae*. *Appl Biochem Biotechnol* 177:541–555. <https://doi.org/10.1007/s12010-015-1761-5>
- Sen TK, Afroze S, Ang HM (2011) Equilibrium, kinetics and mechanism of removal of methylene blue from aqueous solution by adsorption onto pine cone biomass of *Pinus radiata*. *Water Air Soil Pollut* 218:499–515. <https://doi.org/10.1007/s11270-010-0663-y>
- Sen R, Das S, Das K (2011) Effect of stirring rate on the microstructure and microhardness of Ni–CeO₂ nanocomposite coating and investigation of the corrosion property. *Surf Coat Technol* 205:3847–3855. <https://doi.org/10.1016/j.surfcoat.2011.01.057>
- Msaadi R, Sassi W, Hihn J-Y, Ammar S, Chehimi MM (2021) Valorization of pomegranate peel balls as bioadsorbents of methylene blue in aqueous media. *Emergent Mater*. <https://doi.org/10.1007/s42247-021-00174-w>
- Sassi W, Boubaker H, Ben-khaled H, Dhaoui S, Ghorbal A, Hihn J-Y (2021) Modelization and implementation of free adsorption and electrosorption of Cr (VI) from wastewater using Al₂O₃ nanoparticles: assessment and comparison of the two processes. *Environ Sci Pollut Res* 28:28349–28366. <https://doi.org/10.1007/s11356-021-12612-7>
- Lima DR, Lima EC, Thue PS, Dias SLP, Machado FM, Seliem MK, Sher F, Dos Reis GS, Saeb MR, Rinklebe J (2021) Comparison of acidic leaching using a conventional and ultrasound-assisted method for preparation of magnetic-activated biochar. *J Environ Chem Eng* 9:105865. <https://doi.org/10.1016/j.jece.2021.105865>
- Dog M, Alkan M, Onganer Y (2000) Adsorption of methylene blue from aqueous solution onto perlite. *Water Air Soil Pollut* 120:229–248
- Diao Z-H, Xu X-R, Jiang D, Liu J-J, Kong L-J, Li G, Zuo L-Z, Wu Q-H (2017) Simultaneous photocatalytic Cr(VI) reduction and ciprofloxacin oxidation over TiO₂/Fe₀ composite under aerobic conditions: performance, durability, pathway and mechanism. *Chem Eng J* 315:167–176. <https://doi.org/10.1016/j.cej.2017.01.006>
- Sassi W, Mrad M, Behera D, Ammar S, Hihn J-Y (2021) Prediction and optimization of electroplated Ni-based coating composition and thickness using central composite design and artificial neural network. *J Appl Electrochem* 51. <https://doi.org/10.1007/s10800-021-01602-9>
- Pils JRV, Laird DA (2007) Sorption of tetracycline and chlortetracycline on K- and Ca-saturated soil clays, humic substances, and clay–humic complexes. *Environ Sci Technol* 41:1928–1933. <https://doi.org/10.1021/es062316y>
- Ghanmi I, Sassi W, Oulego P, Collado S, Ghorbal A, Díaz M (2022) Optimization and comparison study of adsorption and phosorption processes of mesoporous nano-TiO₂ during discoloration of indigo carmine dye. *Microporous Mesoporous Mater* 342:112138. <https://doi.org/10.1016/j.micromeso.2022.112138>
- Lee W, Kim I, Choi H, Kim K (2013) Synthesis of Ni/NiO core-shell nanoparticles for wet-coated hole transport layer of the organic solar cell. *Surf Coat Technol* 231:93–97. <https://doi.org/10.1016/j.surfcoat.2012.01.024>
- Cai C-B, Han Q-J, Tang L-J, Xu L, Jiang J-H, Wu H-L, Yu R-Q (2009) Studying the uptake of aniline vapor by active alumina through in-line monitoring a differential adsorption bed with near-infrared diffuse reflectance spectroscopy. *Adsorption* 15:23–29. <https://doi.org/10.1007/s10450-008-9146-5>
- Açıklık K (2022) Evaluation of orange and potato peels as an energy source: a comprehensive study on their pyrolysis characteristics and kinetics. *Biomass Convers Biorefinery* 12:501–514. <https://doi.org/10.1007/s13399-021-01387-z>
- Lima DR, Hosseini-Bandegharai A, Thue PS, Lima EC, de Albuquerque YRT, dos Reis GS, Umpierrez CS, Dias SLP, Tran HN (2019) Efficient acetaminophen removal from water and hospital effluents treatment by activated carbons derived from Brazil nutshells. *Colloids Surf A Physicochem Eng Asp* 583:123966. <https://doi.org/10.1016/j.colsurfa.2019.123966>
- Lima EC, Hosseini-Bandegharai A, Moreno-Piraján JC, Anastopoulos I (2019) A critical review of the estimation of the thermodynamic parameters on adsorption equilibria. Wrong use of equilibrium constant in the Van't Hoff equation for calculation of thermodynamic parameters of adsorption. *J Mol Liq* 273:425–434. <https://doi.org/10.1016/j.molliq.2018.10.048>
- Araújo CST, Almeida ILS, Rezende HC, Marcionilio SMLO, Léon JLL, de Matos TN (2018) Elucidation of mechanism involved in adsorption of Pb(II) onto lobeira fruit (*Solanum lycocarpum*) using Langmuir, Freundlich and Temkin isotherms. *Microchem J* 137:348–354. <https://doi.org/10.1016/j.microc.2017.11.009>
- Dos Reis GS, Bergna D, Grimm A, Lima EC, Hu T, Naushad M, Lassi U (2023) Preparation of highly porous nitrogen-doped biochar derived from birch tree wastes with superior dye removal performance. *Colloids Surf. Physicochem Eng Asp* 669:131493. <https://doi.org/10.1016/j.colsurfa.2023.131493>
- Dos Reis GS, Thivet J, Laisné E, Srivastava V, Grimm A, Lima EC, Bergna D, Hu T, Naushad M, Lassi U (2023) Synthesis of novel mesoporous selenium-doped biochar with high-performance sodium diclofenac and reactive orange 16 dye removals. *Chem Eng Sci* 281:119129. <https://doi.org/10.1016/j.ces.2023.119129>
- Lima EC, Dehghani MH, Guleria A, Sher F, Karri RR, Dotto GL, Tran HN (2021) Adsorption: fundamental aspects and applications of adsorption for effluent treatment. In: *Green Technol. Defluoridation Water*. Elsevier, pp 41–88. <https://doi.org/10.1016/B978-0-323-85768-0.00004-X>

28. Lima EC, Hosseini-Bandegharai A, Anastopoulos I Some remarks on a critical review of the estimation of the thermodynamic parameters on adsorption equilibria. Wrong use of equilibrium constant in the van't Hoff equation for calculation of thermodynamic parameters of adsorption—Journal of Molecular Liquids 273 (2019) 425–434. *J Mol Liq* 280(2019):298–300. <https://doi.org/10.1016/j.molliq.2019.01.160>
29. Cunha MR, Lima EC, Lima DR, da Silva RS, Thue PS, Seliem MK, Sher F, dos Reis GS, Larsson SH (2020) Removal of captopril pharmaceutical from synthetic pharmaceutical-industry wastewaters: use of activated carbon derived from *Butia catarinensis*. *J Environ Chem Eng* 8:104506. <https://doi.org/10.1016/j.jece.2020.104506>
30. Msaadi R, Ammar S, Chehimi MM, Yagci Y (2017) Diazonium-based ion-imprinted polymer/clay nanocomposite for the selective extraction of lead (II) ions in aqueous media. *Eur Polym J* 89:367–380. <https://doi.org/10.1016/j.eurpolymj.2017.02.029>
31. Nnadozie EC, Ajibade PA (2020) Data for experimental and calculated values of the adsorption of Pb(II) and Cr(VI) on APTES functionalized magnetite biochar using Langmuir, Freundlich and Temkin equations. *Data Brief* 32:106292. <https://doi.org/10.1016/j.dib.2020.106292>
32. Nnadozie EC, Ajibade PA (2021) Isotherm, kinetics, thermodynamics studies and effects of carbonization temperature on adsorption of indigo carmine (IC) dye using *C. odorata* biochar. *Chem Data Collect* 33:100673. <https://doi.org/10.1016/j.cdc.2021.100673>
33. Jiang H, Hu Q, Cai J, Cui Z, Zheng J, Chen W (2019) Synthesis and dyeing properties of indophenine dyes for polyester fabrics. *Dyes Pigments* 166:130–139. <https://doi.org/10.1016/j.dyepig.2019.03.025>
34. Jiang F, Cao D, Hu S, Wang Y, Zhang Y, Huang X, Zhao H, Wu C, Li J, Ding Y, Liu K (2022) High-pressure carbon dioxide-hydrothermal enhance yield and methylene blue adsorption performance of banana pseudo-stem activated carbon. *Bioresour Technol* 354:127137. <https://doi.org/10.1016/j.biortech.2022.127137>
35. Saadi W, Rodríguez-Sánchez S, Ruiz B, Souissi-Najar S, Ouederni A, Fuente E (2019) Pyrolysis technologies for pomegranate (*Punica granatum L.*) peel wastes. Prospects in the bioenergy sector. *Renew Energy* 136:373–382. <https://doi.org/10.1016/j.renene.2019.01.017>
36. Chen C, Han B, Zhu X, Jiang C, Wang Y (2022) A novel pomegranate peel-derived biochar for highly efficient removal of sulfamethoxazole by activation of peroxydisulfate through a non-radical pathway. *J Environ Chem Eng* 10:108184. <https://doi.org/10.1016/j.jece.2022.108184>
37. Arun KB, Madhavan A, Anoopkumar AN, Surendhar A, Liz Kuriakose L, Tiwari A, Sirohi R, Kuddus M, Rebello S, Kumar Awasthi M, Varjani S, Reshmy R, Mathachan Aneesh E, Binod P, Sindhu R (2022) Integrated biorefinery development for pomegranate peel: prospects for the production of fuel, chemicals and bioactive molecules. *Bioresour Technol* 362:127833. <https://doi.org/10.1016/j.biortech.2022.127833>
38. Guezzen B, Medjahed B, Benhelima A, Guendouzi A, Didi MA, Zidelmal S, Abdelkrim Boudia R, Adjdir M (2023) Improved pollutant management by kinetic and Box-Behnken design analysis of HDTMA-modified bentonite's adsorption of indigo carmine dye. *J Ind Eng Chem* 125:242–258. <https://doi.org/10.1016/j.jiec.2023.05.034>
39. El-Kammah M, Elkhatib E, Gouveia S, Cameselle C, Aboukila E (2022) Enhanced removal of indigo carmine dye from textile effluent using green cost-efficient nanomaterial: adsorption, kinetics, thermodynamics and mechanisms. *Sustain Chem Pharm* 29:100753. <https://doi.org/10.1016/j.scp.2022.100753>
40. Zhou P, Li X, Zhou J, Peng Z, Shen L, Li W (2023) Insights of the adsorption mechanism of methylene blue on biochar from phytoextraction residues of *Citrus aurantium L.*: adsorption model and DFT calculations. *J Environ Chem Eng* 11:110496. <https://doi.org/10.1016/j.jece.2023.110496>
41. Jellali S, Khiari B, Usman M, Hamdi H, Charabi Y, Jeguirim M (2021) Sludge-derived biochars: a review on the influence of synthesis conditions on pollutants removal efficiency from wastewaters. *Renew Sustain Energy Rev* 144:111068. <https://doi.org/10.1016/j.rser.2021.111068>
42. Gao Y, Sinkkonen A, Li H, Oleszczuk P (2022) Advances in agro-environmental organic contamination: an introduction to the Special Issue. *Chemosphere* 287:132071. <https://doi.org/10.1016/j.chemosphere.2021.132071>
43. Zhu X, Sun M, Zhu X, Guo W, Luo Z, Cai W, Zhu X (2023) Molten salt shielded pyrolysis of biomass waste: development of hierarchical biochar, salt recovery, CO₂ adsorption. *Fuel* 334:126565. <https://doi.org/10.1016/j.fuel.2022.126565>
44. Dudziak M, Werle S, Marszałek A, Sobek S, Magdziarz A (2022) Comparative assessment of the biomass solar pyrolysis biochars combustion behavior and zinc Zn(II) adsorption. *Energy* 261:125360. <https://doi.org/10.1016/j.energy.2022.125360>
45. Nguyen BT, Dinh GD, Dong HP, Le LB (2022) Sodium adsorption isotherm and characterization of biochars produced from various agricultural biomass wastes. *J Clean Prod* 346:131250. <https://doi.org/10.1016/j.jclepro.2022.131250>
46. Zhi F, Zhou W, Chen J, Meng Y, Hou X, Qu J, Zhao Y, Hu Q (2023) Adsorption properties of active biochar: overlooked role of the structure of biomass. *Bioresour Technol* 387:129695. <https://doi.org/10.1016/j.biortech.2023.129695>
47. Li H, Kong J, Zhang H, Gao J, Fang Y, Shi J, Ge T, Fang T, Shi Y, Zhang R, Zhang N, Dong X, Zhang Y, Li H (2023) Mechanisms and adsorption capacities of ball milled biomass fly ash/biochar composites for the adsorption of methylene blue dye from aqueous solution. *J Water Process Eng* 53:103713. <https://doi.org/10.1016/j.jwpe.2023.103713>

Publisher's Note Springer Nature remains neutral with regard to jurisdictional claims in published maps and institutional affiliations.

Springer Nature or its licensor (e.g. a society or other partner) holds exclusive rights to this article under a publishing agreement with the author(s) or other rightsholder(s); author self-archiving of the accepted manuscript version of this article is solely governed by the terms of such publishing agreement and applicable law.